

Biomimetic nanoplatform with selectively positioned indocyanine green for accurate sentinel lymph node imaging

Wenjing Cheng^{2,#}, Xiangbai Wu^{1,#}, Shi Yu², Chengwei Zhang², Yinhong Song²,
Xinzhi Li², Xiang Yu^{3,4*}

¹Hubei Provincial Clinical Research Center for Precise Prevention and Treatment of Elderly Gastrointestinal Cancer, The Second People's Hospital of China Three Gorges University, Yichang, China

²Hubei Key Laboratory of Tumor Microenvironment and Immunotherapy, China Three Gorges University, Yichang, China

³School of Biomedical Engineering, Hainan University, Haikou, Hainan, China

⁴Key Laboratory of Biomedical Engineering of Hainan Province, School of Biomedical Engineering, Hainan University

*Corresponding author

*Correspondence to: School of Biomedical Engineering, Hainan University, Haikou, Hainan 570228, China. E-mail addresses: yuxiang@hainanu.edu.cn; yuxiangwl2008@sina.com

#These authors contributed equally to this work

Supporting Information

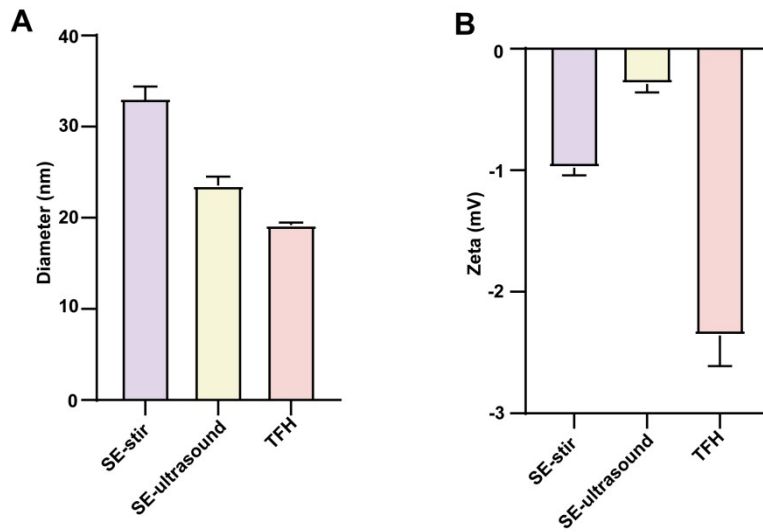


Figure S1: (A) Average size and (B) zeta potential of F127-ICG obtained by the SE and TFH methods. SE: solvent evaporation. TFH: thin film hydration.

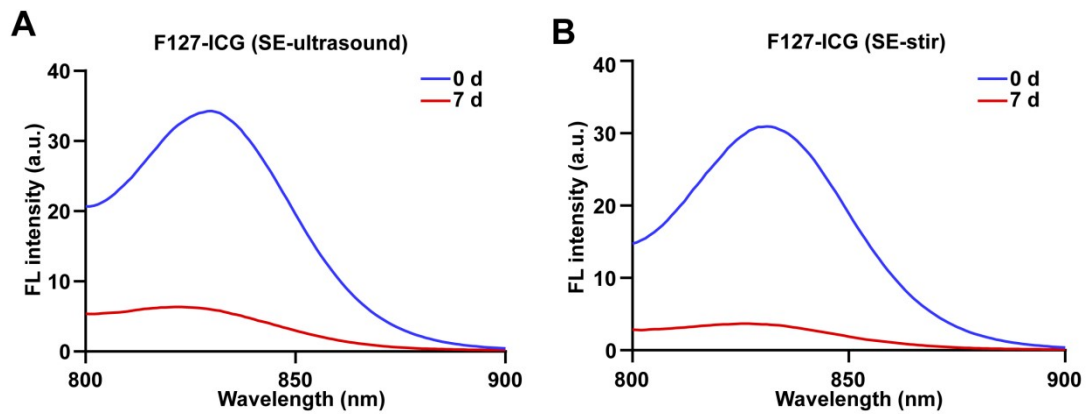


Figure S2: Fluorescence changes of F127-ICG obtained by SE-ultrasound or SE-stir methods at 0 d and 7 d. SE: solvent evaporation.

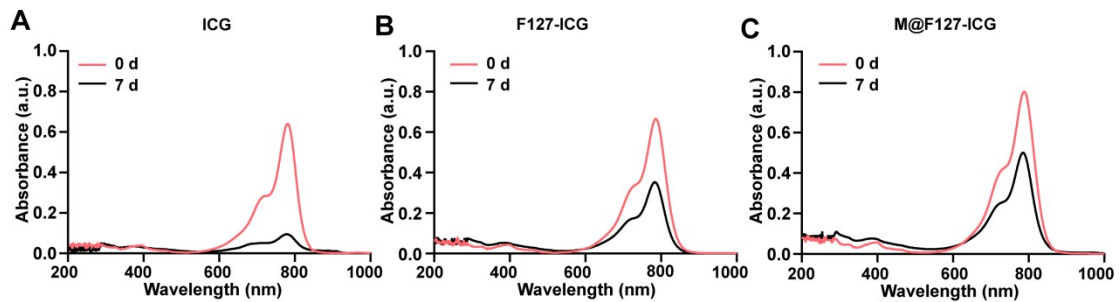


Figure S3: Stability detection of M@F127-ICG. The absorption spectrum of ICG (A), F127-ICG (B), and M@F127-ICG (C) was monitored at 0 d and 7 d.

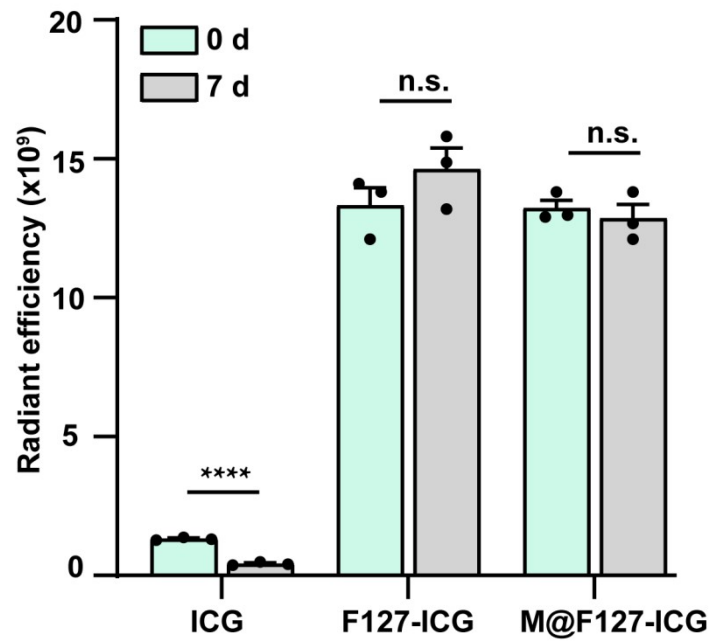


Figure S4: Quantitative analysis of the radiant efficiency in ICG, F127-ICG, and M@F127-ICG in vitro. ICG concentration: 10 μM . Data are presented as the mean \pm SEM and were statistically analysed using unpaired T-tests. n.s. represents no significant difference. **** $p < 0.0001$.

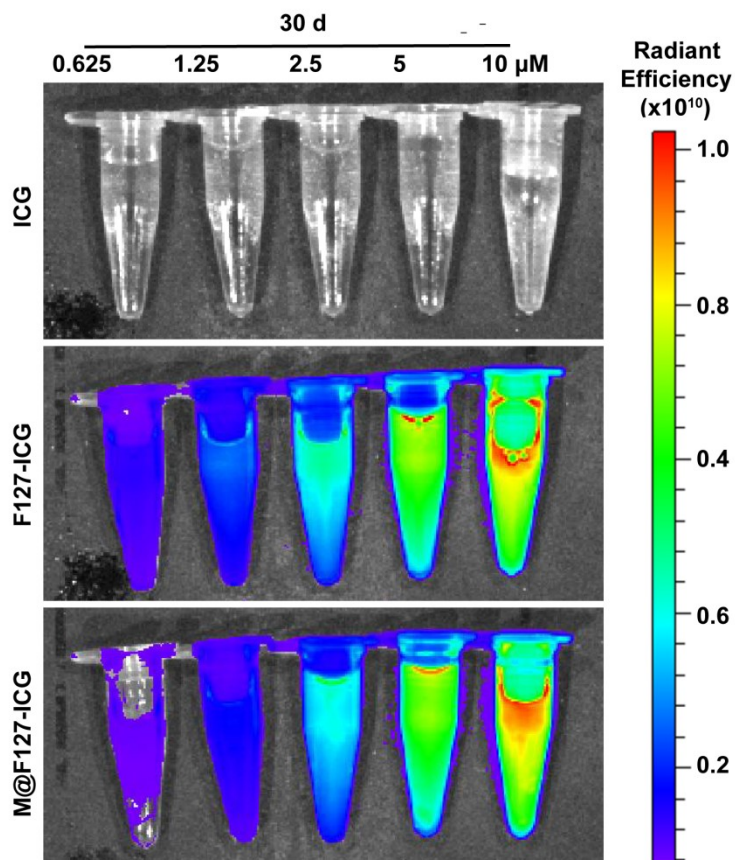


Figure S5: Fluorescence images of ICG, F127-ICG, and M@F127-ICG at 30 d.